Supplementary information to Rheology of MXene-reinforced dual-network hydrogels across swollen and unswollen states

Jiaxin Wu[1], Ruihui Yun[1], Yue Liang[1], Lesen Ma[1,2], Mehdihasan I. Shekh[1], Guangming Zhu[1], Florian Stadler[2,*]

[1] College of Materials Science and Engineering, Shenzhen Key Laboratory of Polymer Science and Technology, Guangdong Research Center for Interfacial Engineering of Functional Materials, Nanshan District Key Laboratory for Biopolymers and Safety Evaluation, Shenzhen University, Shenzhen 518055, P. R. China

[2] Department of Chemical Engineering, Interdisciplinary Research Center for Refining and Advanced Chemicals, King Fahd University of Petroleum and Minerals, Dhahran 31261, Saudi Arabia.

* f.stadler@kfupm.edu.sa

Materials and Synthesis

Table S1：Post-cure gel mass and water content estimated by mass balance.

Sample Name	MX 1 mg/mL aqueous solution (mL)	MX-content/ (ODXT- + CSMA-content) (% (w/w))	Post-cure mass (g)	Water mass (g)	Water mass fraction (wt%）
ODXT@CSMA-DMAm /MX-x	0	0	1.6	0.6230	38.94
	0.03	0.2	1.630	0.6530	40.06
	0.075	0.5	1.675	0.6979	41.64
	0.1.5	1	1.750	0.7729	44.16

TGA

Please note that the high-temperature residue reflects the combined contribution of polymer-derived carbonaceous char (and any inorganic residue from trace salts/impurities) plus the MX-derived inorganic fraction; therefore, the residue is not expected to equal the nominal MX loading.

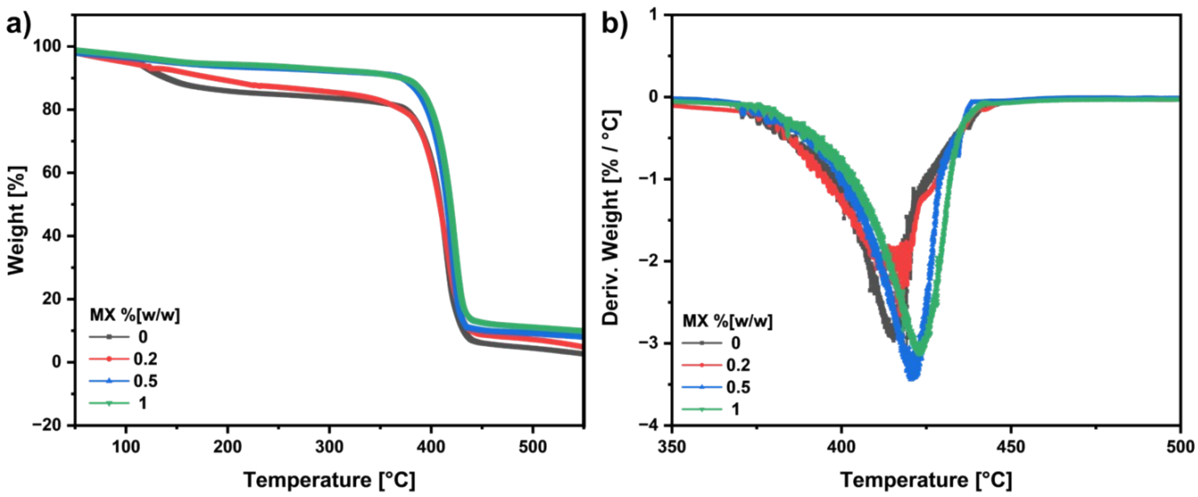

Figure S1: Different MX content of ODXT@CSMA-DMAm/ MX a) TGA curve, b) DTG curve

Normal-force dependence and extrapolation to zero normal force

Oscillatory shear measurements were performed at fixed ω = 10 rad s^{-1} and γ_0 = 0.4% (within the LVE plateau) under applied normal forces F_N = 0.05–0.20 N for all formulations. To quantify potential pre-stress contributions, the storage and loss modulus were fitted as functions of F_N using linear fits in logarithmic scale: $\log_{10}(G')$ = a + bFN. The zero-normal-force modulus were obtained by back-transforming the intercepts, G_0' = 10^a, and is summarized in Table S2. Over the tested range, both G′ and G′′ show only weak dependence on F_N, indicating that the trends with MXene content are not artifacts of normal-force-induced pre-stress. To minimize wall slip during the normal-force series, the sample edges were gently anchored to the plates using a minimal amount of adhesive, and the normal force was monitored throughout the measurements.

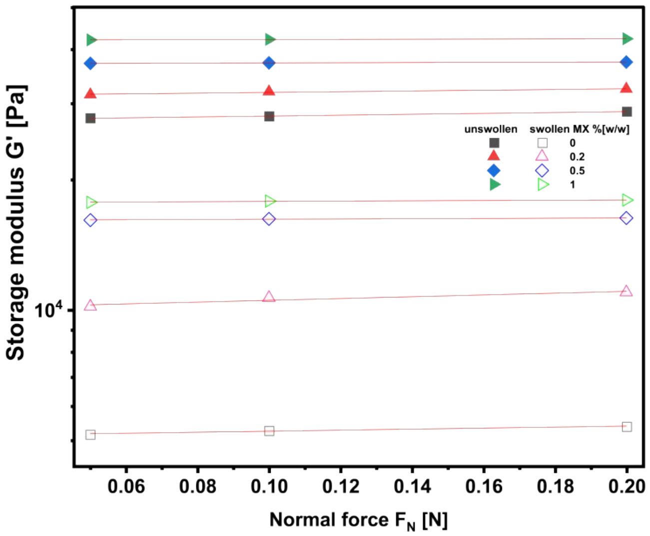

Figure S2: Storage modulus G′ and loss modulus G′′ as a function of applied normal force FN for hydrogels with different MXene contents (w/w relative to ODXT + CSMA), measured at ω=10 rad s−1 and γ = 0.4%. Linear fits of $\log_{10}$ (G′) versus F_N were used to extrapolate modulus to $F_N \rightarrow 0$; the resulting G_0' is summarized in Table S1.

Table S2: Fit parameters for the normal-force dependence of G′ and G′′ and extrapolated zero-normal-force modulus. Fits were performed as $\log_{10}(G')=a + bF_N$.

State	MX-content/(ODXT- + CSMA-content) (% (w/w))	Fit (log10 domain)	Intercept $a=\log_{10}(G_0')$	$G'_0(\text{Pa})=10^a(\text{Pa})$	R^2 (G′)
unswollen	0	$\text{Log}_{10}(G')=4.43777+0.10376*F_N$	4.43777	27401	0.99718
unswollen	0.2	$\text{Log}_{10}(G')=4.49445+0.00227*F_N$	4.49445	31220	0.96035
unswollen	0.5	$\text{Log}_{10}(G')=4.56885+0.02199*F_N$	4.56885	37055	0.99832
unswollen	1	$\text{Log}_{10}(G')=4.62352+0.01701*F_N$	4.62352	42026	0.99339
swollen	0	$\text{Log}_{10}(G')=3.70769+0.11914*F_N$	3.70769	5101	0.97676
swollen	0.2	$\text{Log}_{10}(G')=4.00138+0.20761*F_N$	4.00138	10032	0.90507
swollen	0.5	$\text{Log}_{10}(G')=4.20688+0.00105*F_N$	4.20688	16102	0.92885
swollen	1	$\text{Log}_{10}(G')=4.24737+0.00119*F_N$	4.24737	17675	0.93701

Strain sweep

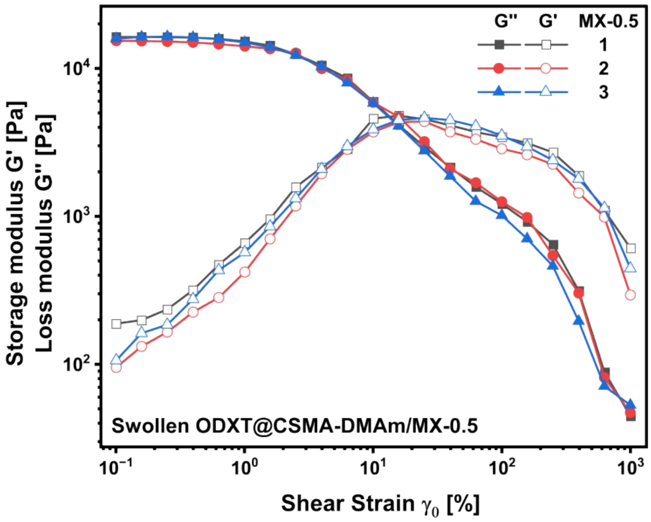

Figure S3: Strain sweep of swollen ODXT@CSMA-DMAm/MX-0.5 hydrogels. three independent replicate samples (1-3) are shown to illustrate the reproducibility of the two-stage nonlinearity trend.

Strain-time sweep

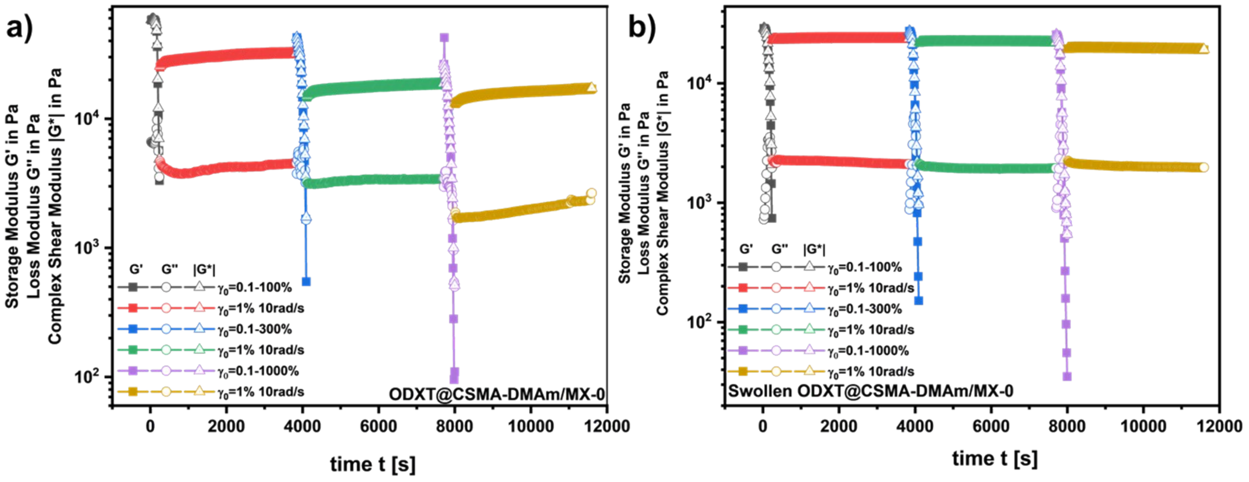

Figure S4: Strain-time sweep of a) ODXT@CSMA-DMAm/MX-0, b) swollen ODXT@CSMA-DMAm/MX-0.

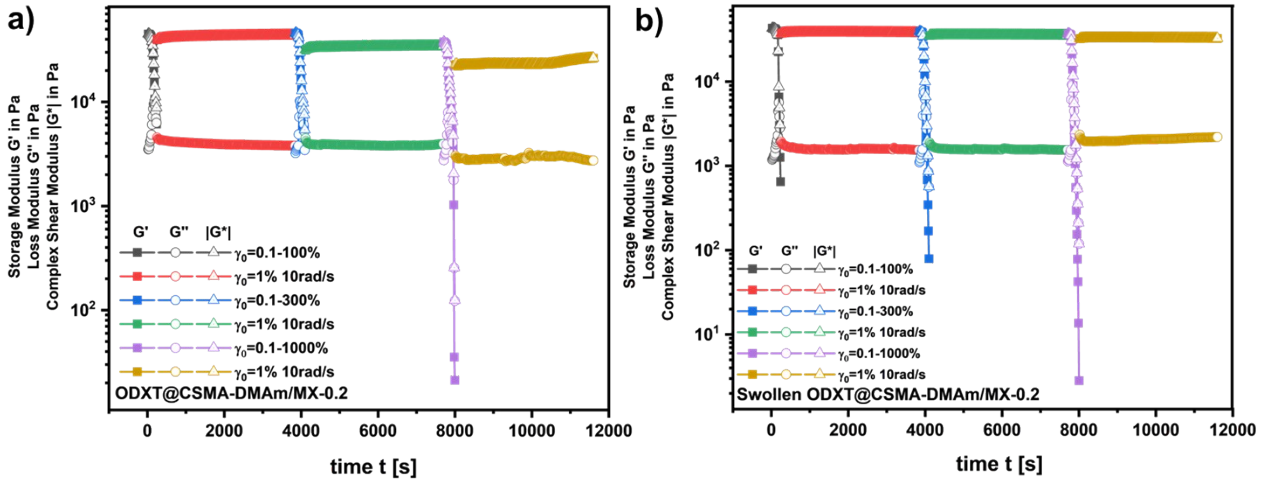

Figure S5: Strain-time sweep of a) ODXT@CSMA-DMAm/MX-0.2, b) swollen ODXT@CSMA-DMAm/MX-0.2.

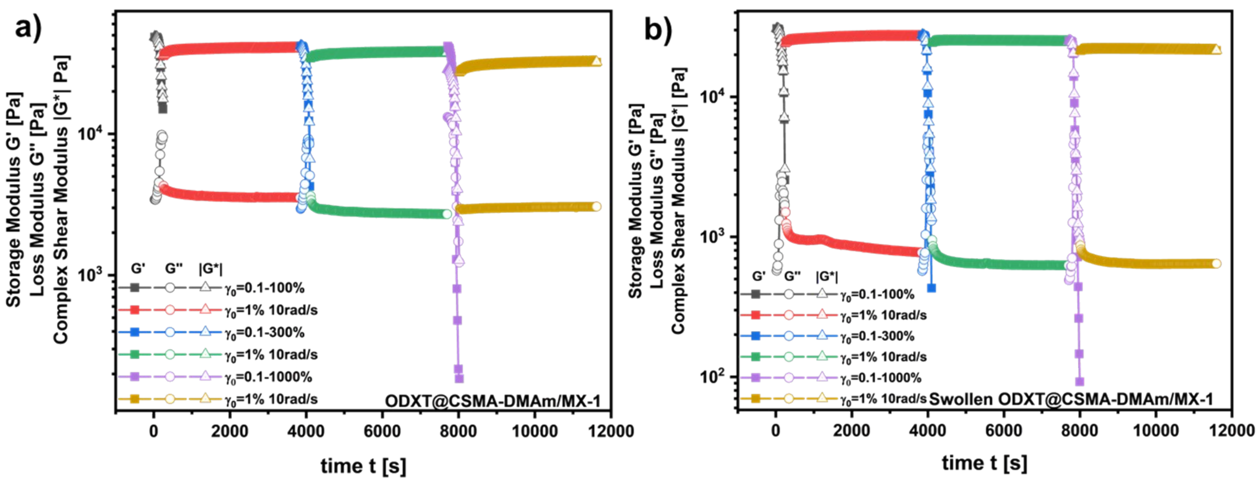

Figure S6: Strain-time sweep of a) ODXT@CSMA-DMAm/MX-1, b) swollen ODXT@CSMA-DMAm/MX-1.

Frequency Sweep

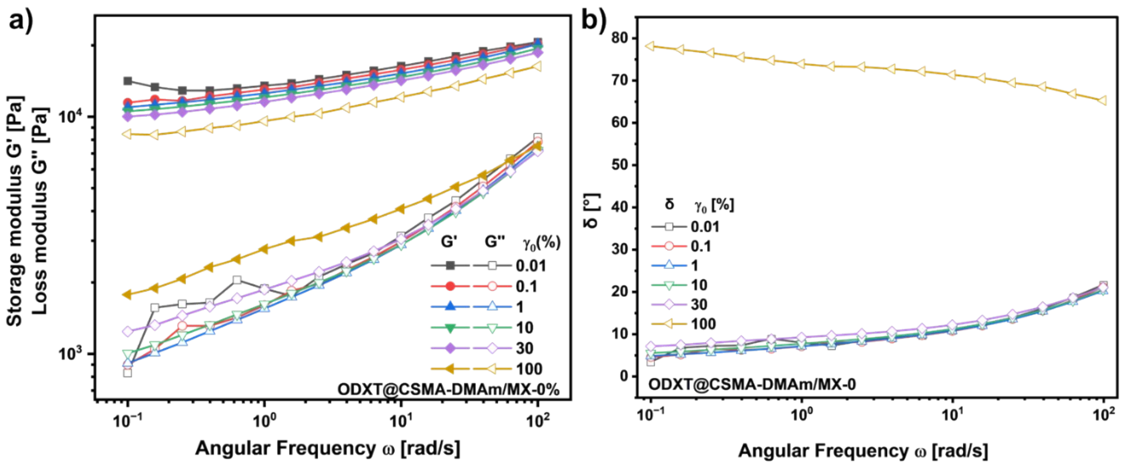

Figure S7: a) Frequency sweeps for ODXT@CSMA-DMAm/MX-0 at different deformation amplitudes and b) Relationship between phase angle and angular frequency.

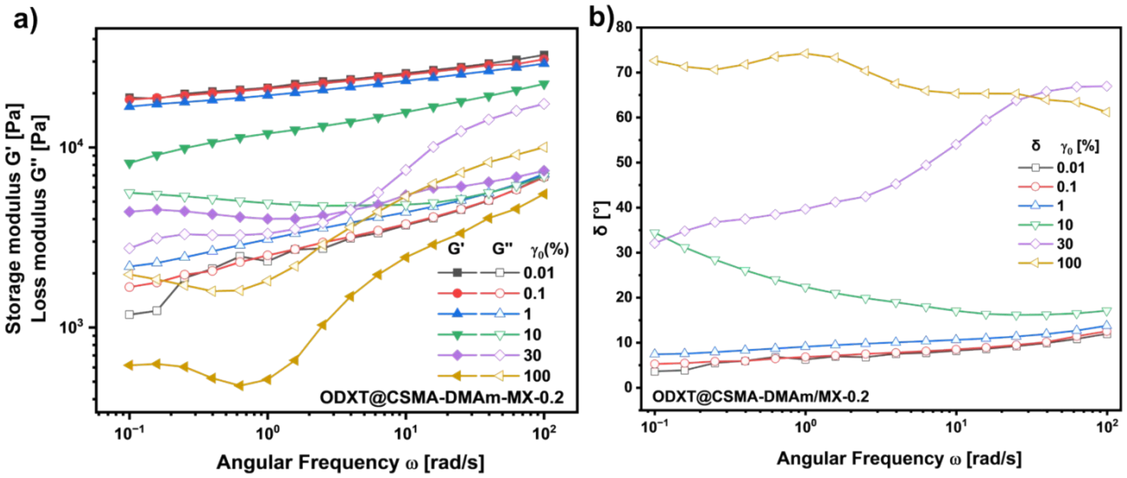

Figure S8: a) Frequency sweeps for ODXT@CSMA-DMAm/MX-0.2 at different deformation amplitudes and b) Relationship between phase angle and angular frequency.

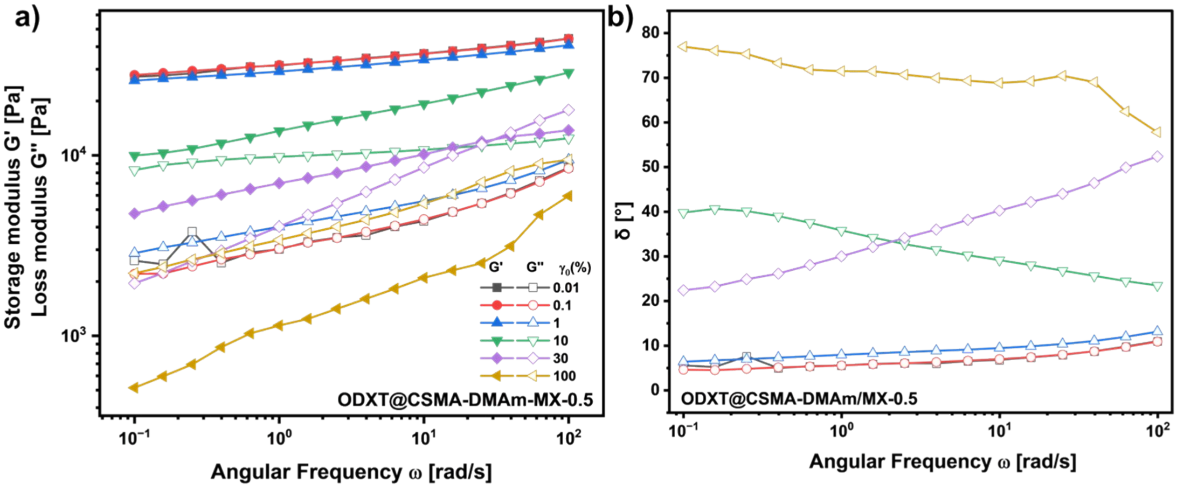

Figure S9: a) Frequency sweeps for ODXT@CSMA-DMAm/MX-0.5 at different deformation amplitudes and b) Relationship between phase angle and angular frequency.

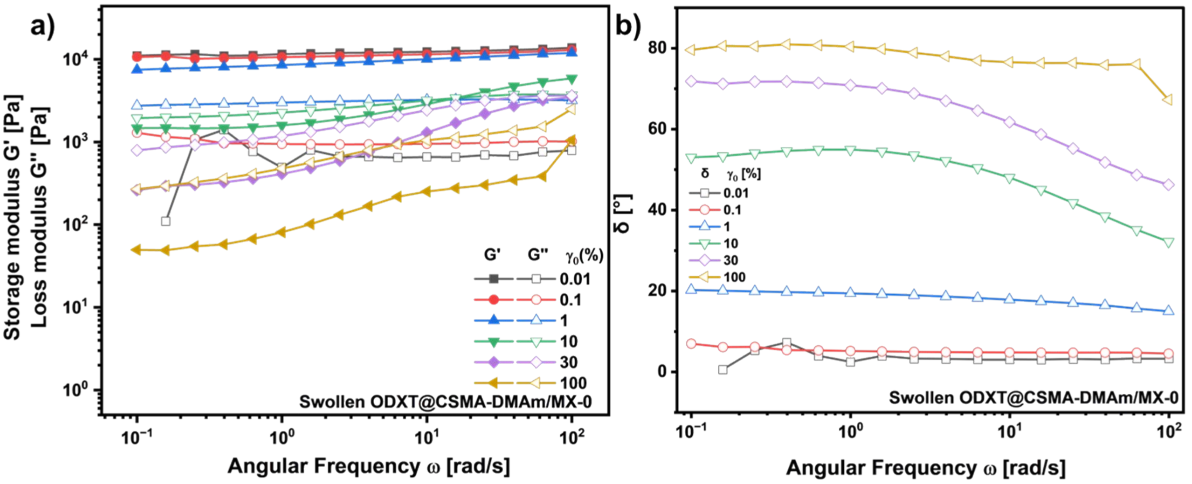

Figure S10: a) Frequency sweeps for swollen ODXT@CSMA-DMAm/MX-0 at different deformation amplitudes and b) Relationship between phase angle and angular frequency.

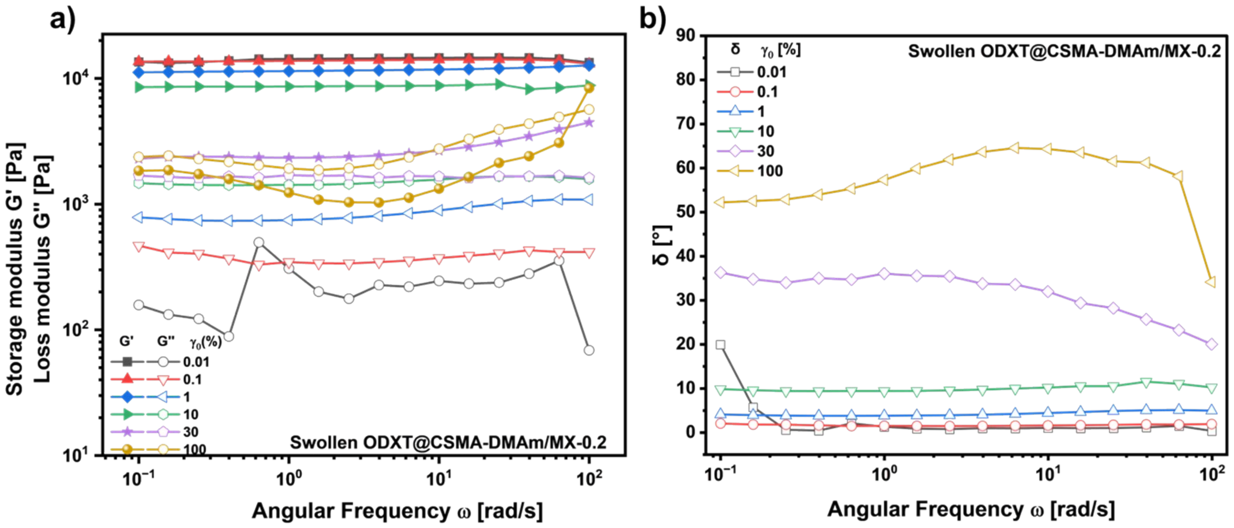

Figure S11: a) Frequency sweeps for swollen ODXT@CSMA-DMAm/MX-0.2 at different deformation amplitudes and b) Relationship between phase angle and angular frequency.

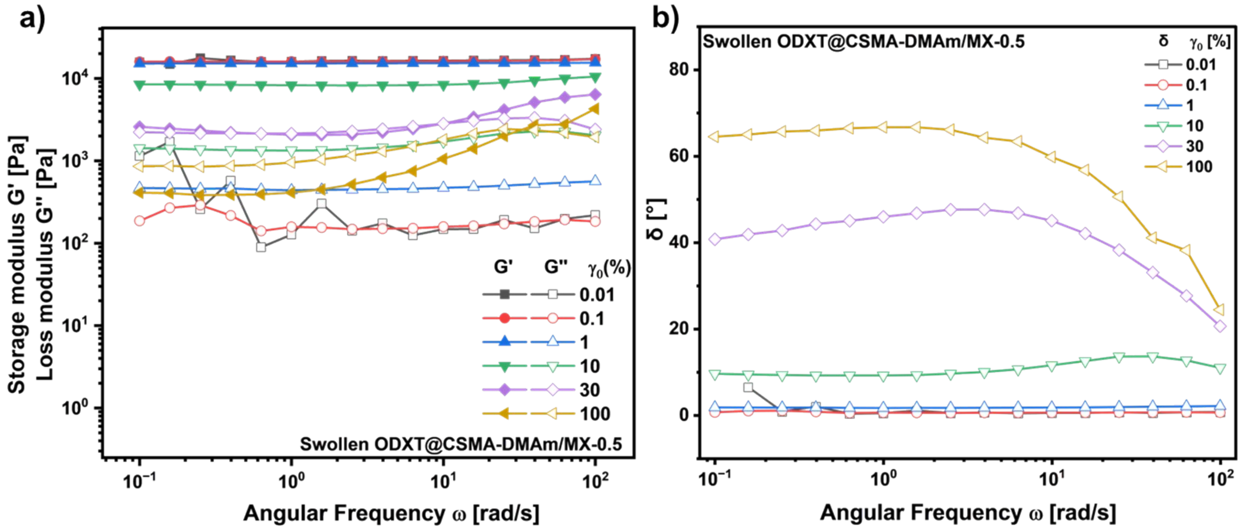

Figure S12: a) Frequency sweeps for swollen ODXT@CSMA-DMAm/MX-0.5 at different deformation amplitudes and b) Relationship between phase angle and angular frequency.

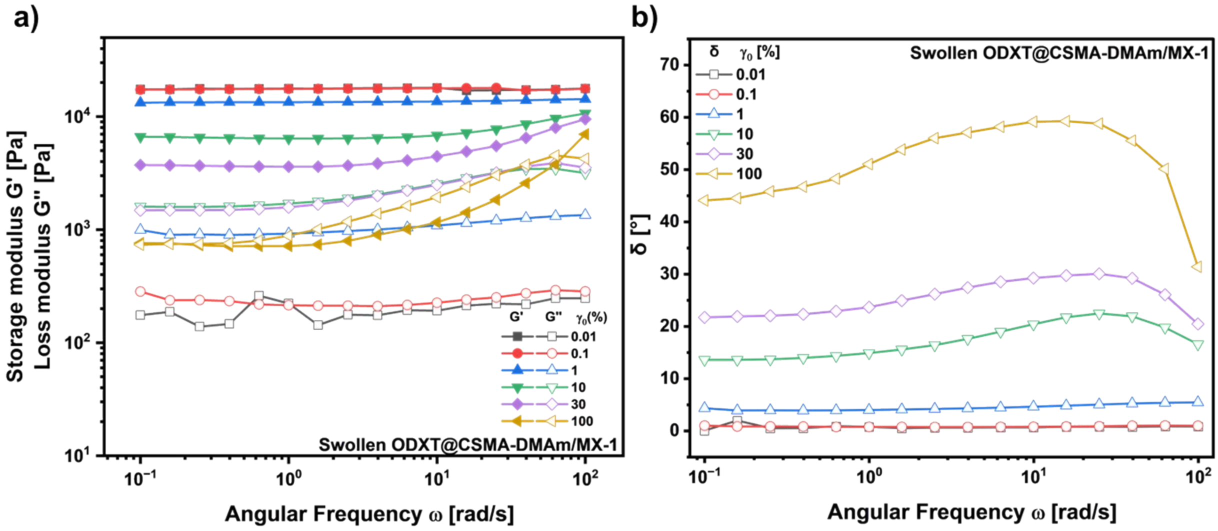

Figure S13: a) Frequency sweeps for swollen ODXT@CSMA-DMAm/MX-1 at different deformation amplitudes and b) Relationship between phase angle and angular frequency.

Extensional rheology

Figure S14: Photograph of the dual-pin grip configuration used for uniaxial extensional testing. Strip specimens were mounted by wrapping each end around a cylindrical post to provide frictional anchoring and to minimize slip. The gauge section was defined as the free span between the two posts.

XRD

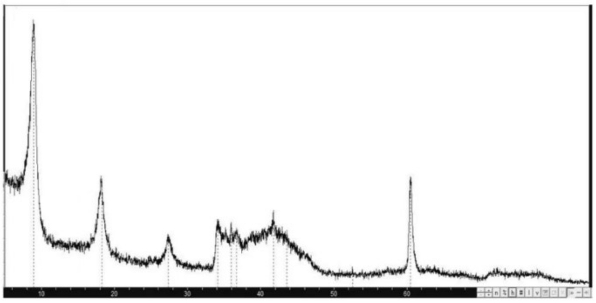

Figure S15: Supplier-provided XRD pattern of the as-received $Ti_3C_2T_x$ *MXene, included as supporting documentation for the purchased material.*